Title

Quantitative MRI biomarker for classification of clinically significant prostate cancer: Calibration for reproducibility across echo times.

Journal

Journal of Applied Clinical Medical Physics, 25(11)

Authors

Kallis, Karoline

Conlin, Christopher

Ollison, Courtney

et al.

Publication Date

2024-11-01

DOI

10.1002/acm2.14514

Peer reviewed

Received: 12 February 2024 | Revised: 8 August 2024 | Accepted: 14 August 2024

DOI: 10.1002/acm2.14514

JOURNAL OF APPLIED CLINICAL MEDICAL PHYSICS

IMAGING PHYSICS

Quantitative MRI biomarker for classification of clinically significant prostate cancer: Calibration for reproducibility across echo times

Karoline Kallis[1] | **Christopher C. Conlin**[2] | **Courtney Ollison**[1] | **Michael E. Hahn**[2] | **Rebecca Rakow-Penner**[2] | **Anders M. Dale**[2,3,4] | **Tyler M. Seibert**[1,2,5]

[1]Department of Radiation Medicine and Applied Sciences, UC San Diego Health, La Jolla, California, USA

[2]Department of Radiology, UC San Diego Health, La Jolla, California, USA

[3]Department of Neurosciences, UC San Diego Health, La Jolla, California, USA

[4]Halıcıoğlu Data Science Institute, UC San Diego, La Jolla, California, USA

[5]Department of Bioengineering, UC San Diego Jacobs School of Engineering, La Jolla, California, USA

Correspondence
Tyler Seibert, Department of Radiation Medicine & Applied Sciences, UC San Diego Health, 3855 Health Sciences Drive, La Jolla, CA 92093-0843, USA.
Email: tseibert@ucsd.edu

Anders M. Dale and Tyler M. Seibert are co-senior authors.

Funding information
National Institutes of Health, Grant/Award Numbers: NIH/NIBIB K08EB026503, NIH UL1TR000100; American Society for Radiation Oncology; Prostate Cancer Foundation; Department of Defense, Grant/Award Number: DOD/CDMRP PC220278

Abstract

Purpose: The purpose of the present study is to develop a calibration method to account for differences in echo times (TE) and facilitate the use of restriction spectrum imaging restriction score (RSIrs) as a quantitative biomarker for the detection of clinically significant prostate cancer (csPCa).

Methods: This study included 197 consecutive patients who underwent MRI and biopsy examination; 97 were diagnosed with csPCa (grade group ≥ 2). RSI data were acquired three times during the same session: twice at minimum TE ~75 ms and once at TE = 90 ms ($TEmin_1$, $TEmin_2$, and TE90, respectively). A linear regression model was determined to match the C-maps of TE90 to the reference C-maps of $TEmin_1$ within the interval ranging from 95th to 99th percentile of signal intensity within the prostate. RSIrs comparisons were made at the 98th percentile within each patient's prostate.

We compared RSIrs from calibrated TE90 ($RSIrs_{TE90corr}$) and uncorrected TE90 ($RSIrs_{TE90}$) to RSIrs from reference $TEmin_1$ ($RSIrs_{TEmin1}$) and repeated $TEmin_2$ ($RSIrs_{TEmin2}$). Calibration performance was evaluated with sensitivity, specificity and area under the ROC curve (AUC).

Results: Scaling factors for C_1, C_2, C_3, and C_4 were estimated as 1.68, 1.33, 1.02, and 1.13, respectively. In non-csPCa cases, the 98th percentile of $RSIrs_{TEmin2}$ and $RSIrs_{TEmin1}$ differed by 0.27 ± 0.86SI (mean ± standard deviation), whereas $RSIrs_{TE90}$ differed from $RSIrs_{TEmin1}$ by 1.82 ± 1.20SI. After calibration, this bias was reduced to -0.51 ± 1.21SI, representing a 72% reduction in absolute error. For patients with csPCa, the difference was 0.54 ± 1.98SI between $RSIrs_{TEmin2}$ and $RSIrs_{TEmin1}$ and 2.28 ± 2.06SI between $RSIrs_{TE90}$ and $RSIrs_{TEmin1}$. After calibration, the mean difference decreased to -1.03SI, a 55% reduction in absolute error. At the Youden index for patient-level classification of csPCa (8.94SI), $RSIrs_{TEmin1}$ has a sensitivity of 66% and a specificity of 72%.

Conclusions: The proposed linear calibration method produces similar quantitative biomarker values for acquisitions with different TE, reducing TE-induced error by 72% and 55% for non-csPCa and csPCa, respectively.

KEYWORDS
calibration, diffusion-weighted imaging, echo time, prostate cancer, quantitative biomarker, restricted spectrum imaging restriction score

1 | INTRODUCTION

Around 288,300 new cases of prostate cancer were expected in the United States in 2023 alone, accounting for nearly 29% of all cancer cases in men.[1] The standard procedure to diagnose clinically significant prostate cancer (csPCa) includes multiparametric MRI (mpMRI) prior to biopsy.[2] A biopsy is an expensive and invasive procedure, which has the potential for both overdiagnosis and underdiagnosis of csPCa, given that only a small part of the prostate gland[2] is sampled, which is why accurate imaging of the whole prostate gland is valuable. A large percentage of men suspected to have csPCa can be safely reassured without biopsy if the prostate gland appears normal on mpMRI, and further, when a biopsy is needed, needles can be directed to the most suspicious lesions.

Diffusion-weighted imaging (DWI) plays a crucial role in mpMRI for the detection and characterization of csPCa.[3] Commonly, the apparent diffusion coefficient (ADC) is evaluated to identify csPCa. However, ADC is a simplification of the diffusion process, ignoring non-Gaussian restricted diffusion, and hence does not accurately represent the tumor properties.[4] More advanced DWI models have been designed to better represent the microstructure of real tissue. Examples include intravoxel incoherent motion imaging,[5,6] diffusion kurtosis imaging,[7,8] vascular, extracellular, and restricted diffusion for cytometry in tumor (VERDICT),[9–11] hybrid multidimensional MRI,[12–15] and restriction spectrum imaging (RSI).[9,16]

In the case of RSI, the overall diffusion signal is represented as a weighted combination of signal contributions from multiple tissue compartments, each characterized by a different, fixed diffusion coefficient.[16,17] Prior studies have developed and validated a four-compartment model for prostate cancer detection, with compartments corresponding broadly to restricted, hindered, and free diffusion, plus vascular flow.[17–20] The biomarker RSI restriction score (RSIrs) is derived by normalizing the signal from the model coefficient of the most restricted diffusion compartment (referred to as C_1) by the median T_2-weighted signal intensity within the prostate. RSIrs has proven to be a valuable biomarker for identifying csPCa,[17–19] demonstrating superior detection of csPCa compared to ADC, and similar performance to that of PI-RADS v2.1.[18,19] However, acquisition parameters like echo time (TE) can influence the quantitative value of RSIrs.[21]

To maximize the utility of RSIrs as a quantitative biomarker, we propose a simple calibration method, based on MRI biophysics, for data obtained at varying TE values. We demonstrate a partial linear relationship between RSIrs and TE and compare RSIrs values at two different TEs before and after calibration. By addressing the challenge of TE-dependent variability, we aim to advance the potential of mpMRI as a valuable clinical tool in the diagnosis and management of prostate cancer.

2 | MATERIALS AND METHODS

2.1 | Patient cohort

This study was conducted under the approval of the institutional review board at UC San Diego (IRB 210213) with a waiver of consent for prospective collection of RSI at multiple TEs. The research adhered to the principles outlined in the Declaration of Helsinki and all relevant regulations. 218 consecutive patients who underwent MRI examinations between 03/2021 and 02/2023 were included in the study. Patients were excluded from the study if they had undergone prior treatment for prostate cancer, had a hip implant, or had a PI-RADS score greater than 1 and no available biopsy result was performed within 182 days of MRI acquisition. Further, patients were excluded because one of the TE acquisitions was missing, the imaging protocol did not match the norm for this analysis, or the pathology report was inconclusive. In total, 197 patients were included in the study. 97 of the 197 patients were identified to have csPCa, while 100 had only benign tissue or grade group 1 cancer. Further details of the patient cohort are presented in Table 1.

MRI examinations were interpreted per routine clinical practice by ten board-certified and subspecialty fellowship-trained radiologists. 38 of the 197 scans were part of a separate research study for evaluation of treatment response and did not have an official clinical interpretation but did have proven high-grade csPCa on biopsy, with MRI-visible lesions defined on prior clinical scans by a board-certified radiologist (max 6 months prior) and confirmed on the research scan by a subspecialist radiation oncologist and prostate MRI scientist (10 years of experience). Segmentation of the whole prostate was performed using an FDA-cleared commercial AI tool (OnQ Prostate, Cortechs Labs, San Diego, CA, USA). Biopsy (systematic and targeted) and prostatectomy were conducted in accordance with clinical protocols, and both were examined by board-certified pathologists. Clinically significant prostate cancer

TABLE 1 Patient characteristics

Parameter	Specification	Value
Number of patients	Total	197
#patients with Urolift	Total	3
Recruiting time frame	Range	03/2021–02/2023
Age [a]	Median (IQR)	69 (10)
Time from MRI to biopsy [d]	Median (IQR)	56 (72)
PSA at time of MRI [ng/mL]	Median (IQR)	6.0(5.1)
Prostate volume [mL]	Median (IQR)	49 (37)
PSA density [ng/mL^2]	Median (IQR)	0.11 (0.11)
Biopsy naïve	Yes	44
	No	44
	Unknown	109
Best available pathology	Systematic only	73
	Targeted only	2
	Systematic + Targeted	76
	No biopsy	37
	Unknown biopsy type	9
	Prostatectomy	23
PI-RADS score	1	68
	2	10
	3	18
	4	34
	5	29
	No score	38
Gleason grade group	Benign	72
	1	28
	2	41*
	3	31*
	4	8*
	5	17*

Abbreviations: IQR = inter quartile range; MRI = magnet resonance imaging; PSA = prostate-specific antigen.
*clinically significant prostate cancer.

(csPCa) was defined as grade group ≥ 2. In cases where patients underwent prostatectomy, the determination of the grade group was based on the final pathology report.

2.2 | MRI acquisition

All MRI acquisitions were carried out on a 3T clinical GE scanner (Discovery MR750, GE Healthcare, Waukesha, WI, USA), using a 32-channel phased-array body coil encompassing the pelvis. The acquisition parameters can be found in Table 2. For all patients, three axial RSI scans were obtained each sampled five *b*-values (0, 50, 800, 1500, 3000 s/mm^2). Two of the scans were acquired with minimum echo time (TEmin$_1$ and TEmin$_2$, approximately 75 ms), and the third series was acquired with an echo time (TE) of 90 ms (TE90). A high-resolution T_2-weighted reference image was also acquired with the field of view (FOV) identical to the RSI volumes.

Postprocessing of the image data was performed using in-house software in MATLAB (version R2017a, MathWorks, Natick, MA, USA). DWI images were corrected for B_0 inhomogeneity distortions, gradient nonlinearity, and eddy currents.[20,22,23] Multiple acquired DWI samples at specific *b*-values were averaged together and normalized by the median signal intensity of urine in the bladder at $b = 0$ s/mm^2. RSI model fitting was performed as described in prior studies.[17–19]

2.3 | RSIrs: quantitative biomarker

The RSI model is defined by the following formal:

$$S_{\text{corr}}(b) = \sum_{i=1}^{K} C_i e^{-bD_i} \quad (1)$$

$S_{\text{corr}}(b)$ defines the acquired averaged and noise-corrected DWI image at a particular *b*-value. D_i is the compartmental ADC. K denotes the number of tissue compartments. For this study, we modeled the signal using a four-compartment approach. C_i is the unitless weighting factor describing the contribution of a particular compartment to the overall signal. The first compartment (C_1) describes the signal from the slowest (intracellular restricted) compartment.[17,20]

The biomarker RSIrs is defined as C_1, normalized by the median signal intensity of the prostate at a *b*-value of 0s/mm^2 (*mb0*), that is, the median T_2-weighted signal of the whole prostate.

$$\text{RSIrs}_j = \frac{C_{1j}}{mb0} \quad (2)$$

where *j* defines a voxel. Our emphasis was on high percentiles of RSIrs within the prostate, as the highest RSIrs values within each prostate are utilized for identifying csPCa on a patient level.[19] In this study, RSIrs comparisons were made at 98th percentile within each patient's prostate, as this is expected to be more stable than the maximum voxel and thus more robustly calibrated. For better display in medical imaging software, RSIrs has been multiplied by 100.

2.4 | Calibration concept

Our hypothesis is that there exists a partial linear, echo-time dependent relationship among the acquired RSIrs-maps, as expressed in Equation (3):

$$S_{\text{corr}}(b) = \sum_{i=1}^{K} C_i e^{-bD_i} * e^{-\frac{\text{TE}}{\text{T2}}} \quad (3)$$

where T_2 defines the coefficient defining the T_2-effect observed in the acquired images and TE the used echo

TABLE 2 Acquisition parameters for clinical multiparametric MRI.

Series	RSI—TEmin	RSI—TE90	T2W
FOV [mm]	200 × 100	200 × 100	200 × 200
Matrix (resampled dimensions)	80 × 48 (128 × 128)	80 × 48 (128 × 128)	320 × 320 (512 × 512)
Number of slices	32	32	32
Pixel size [mm	1.56 × 1.56	1.56 × 1.56	
Slice thickness [mm]	3	3	3
TR [ms]	4500	4500	6176
TE [ms]	75.6–76.3	90	106
b-values [s/mm^2](number of samples)	0 (1), 50 (6), 800 (6), 1500 (12), 3000 (18)	0 (1), 50 (6), 800 (6), 1500 (12), 3000 (18)	N/A

Abbreviations: RSI = restriction spectrum imaging; T_2W = T2 weighted MRI.

time. As a demonstration of the concept, a linear regression model was optimized to partially fit RSIrs of TE90 to match RSIrs of $TEmin_1$ within the range from the 95th to the 99th percentile of signal intensity within the prostate. By limiting the fitting to the range of high percentiles the influence of noisy data and imaging artifacts was minimized. Further, we focused on high percentiles of RSIrs because the highest values of RSIrs within each prostate are used to detect the presence of csPCa on a patient level. As a result, linear scaling factors (f) were determined for each diffusion compartment (C), however, currently, only the information of C_1 is included in RSIrs. Further, to ensure standardization, a calibrated *mb0* value was determined for normalization purposes. The calibration of *mb0* involved the artificial generation of DWI, utilizing the estimated scaling factors. This process effectively replicated the acquisition conditions with reference TE, see Figure S1.

Data from 100 control subjects (without csPCa) were used for training a partial linear regression model. The model was validated on the training set and a testing set comprised of 97 subjects with csPCa. To determine the minimal amount of training data required for reliable results, we calculated the scaling factors using different sample sizes, starting with a minimum of 10% of the total dataset. The subsets of samples were randomly selected and fitted 1000 times to account for patient variability.

2.5 | Data analysis

The 98th percentile of RSIrs values within the whole prostate were compared between the reference $TEmin_1$ ($RSIrs_{TEmin1}$) scan and the TE90 ($RSIrs_{TE90}$) scan, the $TEmin_2$ ($RSIrs_{TEmin2}$) scan, and the TE90 scan after calibration ($RSIrs_{TE90corr}$). The difference between $RSIrs_{TEmin2}$ and $RSIrs_{TEmin1}$, acquired within minutes of each other with the same echo time, delineates the best achievable calibration and defines the error between various acquisitions with the same imaging parameters.

The mean and standard deviation of the differences in the 98th percentile within each patient's prostate between $RSIrs_{TEmin1}$ and $RSIrs_{TE90}$, $RSIrs_{TEmin2,}$ and $RSIrs_{TE90corr}$ were analyzed. A negative mean value describes that the quantitative value of the reference $RSIrs_{TEmin1}$ acquisitions is higher than the corresponding RSIrs-map. A paired t-test of the 98th percentiles between varying TE acquisitions was used to test for statistical significance ($p < 0.05$).

Statistical performance of the calibration was investigated by comparing the sensitivity, and specificity at a specific threshold (Youden index based on the ROC curve for $RSIrs_{TEmin1}$).

3 | RESULTS

Scaling factors for C_1, C_2, C_3, and C_4-maps were estimated at 1.68, 1.33, 1.02, and 1.13, respectively, for converting TE90 data to the TEmin reference. Examples illustrating cases are presented in Figure 1 (absence of csPCa) and Figure 2 (presence of csPCa). Our analysis revealed that a minimum of around 35 patients would be required to reproduce a comparable calibration for different scanners or disease sites (see Figure S5A).

Figure 3 illustrates the 98th percentile of $RSIrs_{TE90}$, $RSIrs_{TE90corr}$, and $RSIrs_{TEmin2}$ within the prostate for each patient, comparing them to the reference (98th percentile of $RSIrs_{TEmin1}$). In non-csPCa cases, a difference of 0.27 ± 0.86SI ($p < 0.01$) was observed between the 98th percentiles of $RSIrs_{TEmin2}$ and $RSIrs_{TEmin1}$. The difference between $RSIrs_{TE90}$ and $RSIrs_{TEmin1}$ was 1.82 ± 1.20SI ($p < 0.01$), indicating that a ~15 ms change in TE led to a 7-fold increase in the difference between RSIrs measurements, compared to a repeat acquisition at the same TE. Following calibration, however, the bias between the two series was reduced to -0.51SI ($p < 0.01$), representing a 72% reduction in absolute error. In patients with csPCa, the 98th percentile of RSIrs differed by 0.54 ± 1.98SI ($p < 0.01$) between $RSIrs_{TEmin2}$ and $RSIrs_{TEmin1}$. Prior to cali-

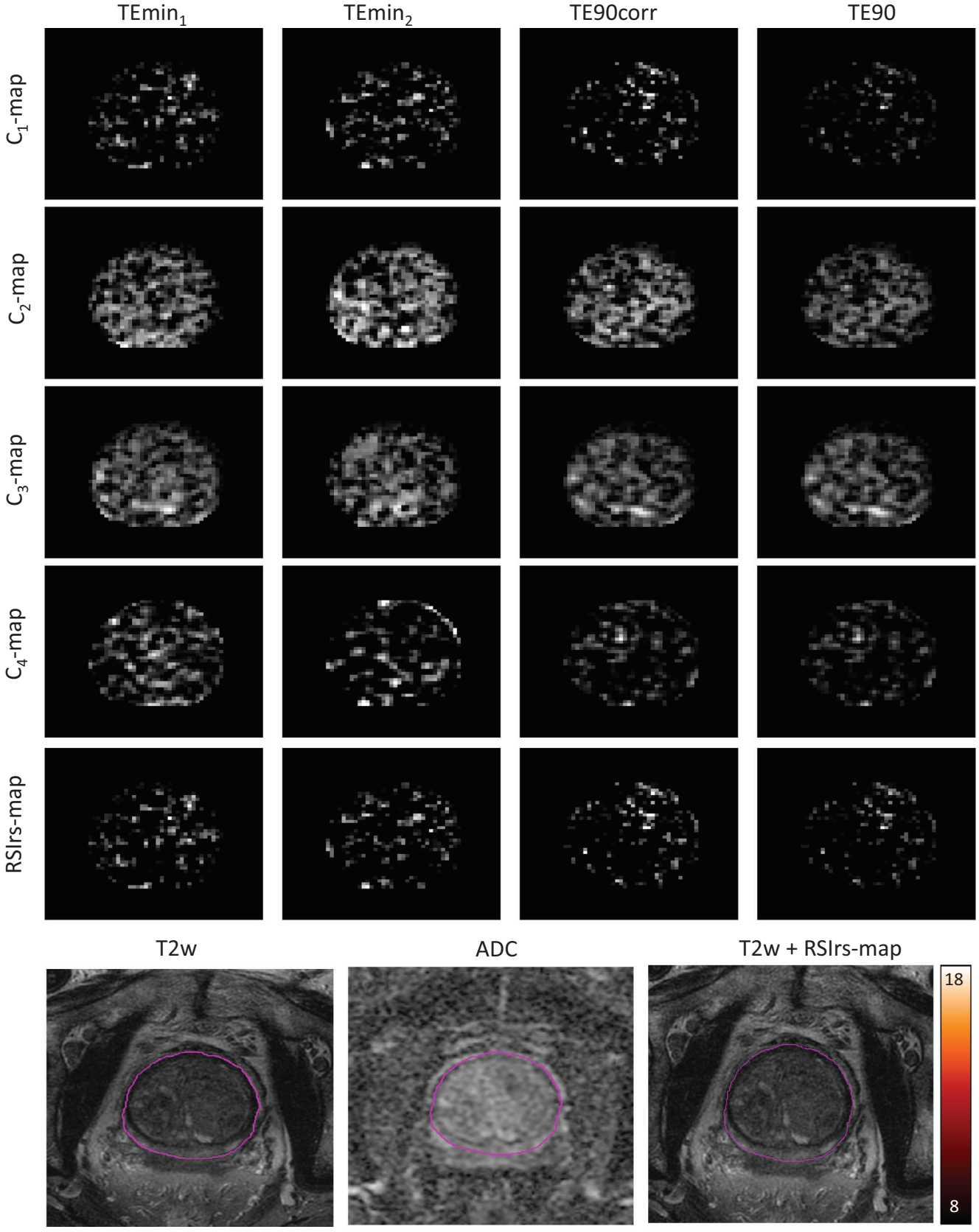

FIGURE 1 C-maps and RSIrs-maps for a patient without csPCa. Images are shown for the $TEmin_1$, $TEmin_2$, TE90, and TE90corr acquisitions. The bottom row shows the corresponding T2w image, the ADC map, as well as an overlay of the RSIrs-map with T2w- images. Color bar: RSIrs; Pink contours: prostate gland. ADC = apparent diffusion coefficient; csPCa =clinically significant prostate cancer.

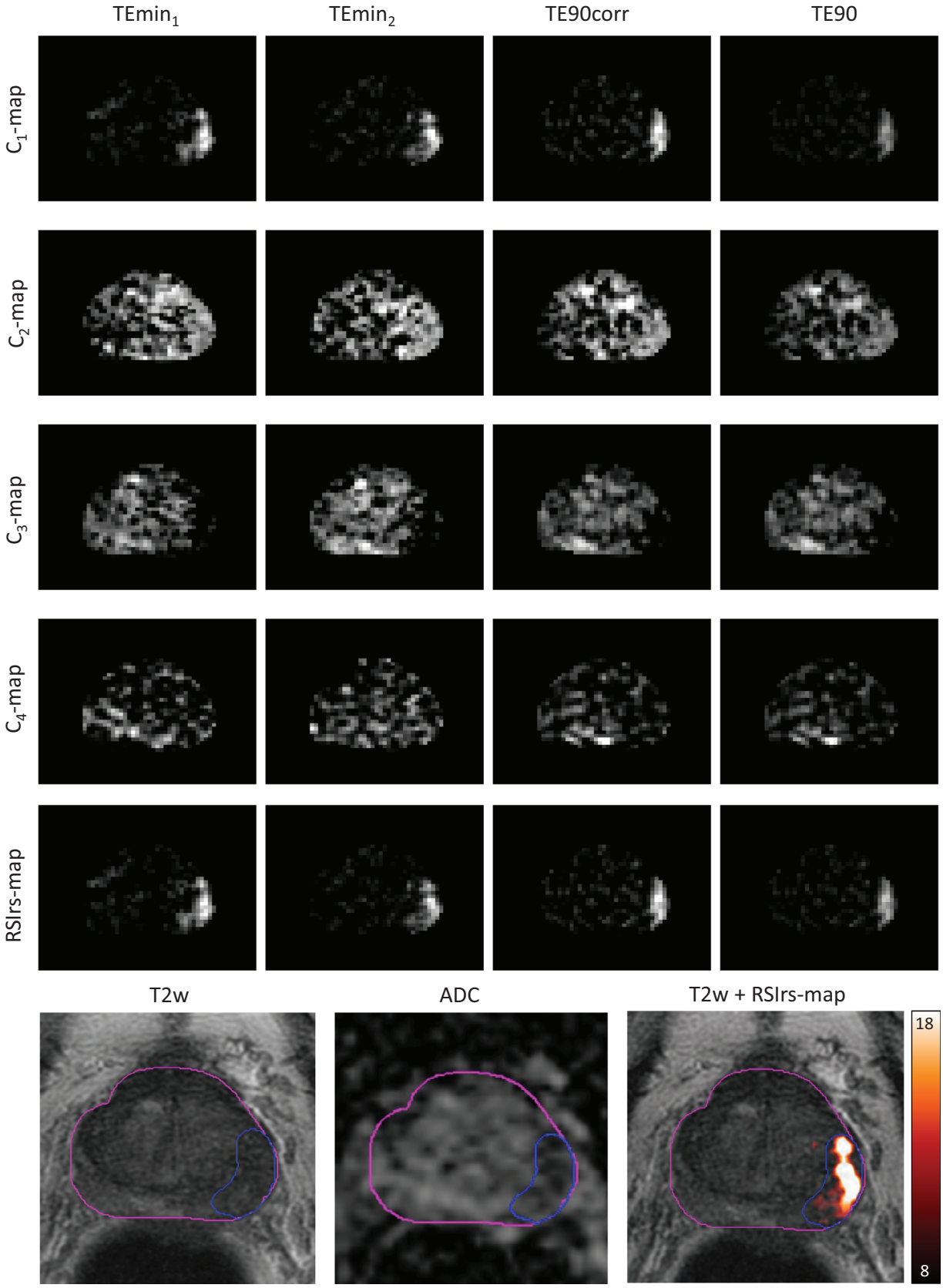

FIGURE 2 C-maps and RSIrs-maps for a patient with csPCa (PI-RADS 5 lesion). Images are shown for the $TEmin_1$, $TEmin_2$, TE90, and TE90corr acquisitions. The bottom row shows the corresponding T2w image, the ADC map, as well as an overlay of RSIrs-map and T2w image. Color bar: RSIrs; Pink contours: prostate gland; blue contour: biopsy-proven csPCa lesion (PI-RADS 5). ADC = apparent diffusion coefficient; csPCa =clinically significant prostate cancer.

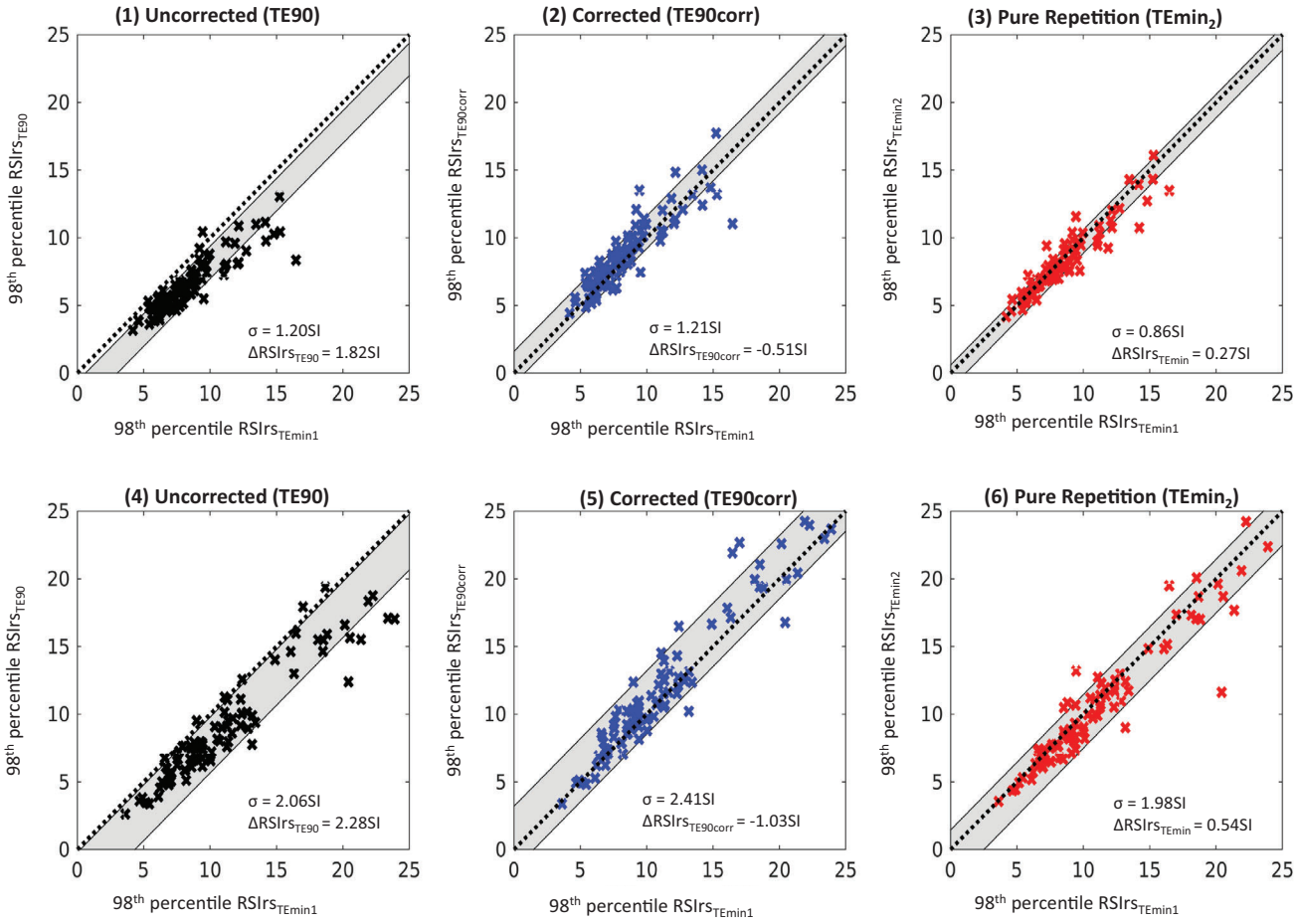

FIGURE 3 Comparison of the 98th percentile of $RSIrs_{TEmin1}$ to that of $RSIrs_{TE90}$ for benign cases (1–3) and csPCa (4–6) cases, for the $RSIrs_{TE90}$ (1, 4), $RSIrs_{TE90corr}$ (2, 5) and $RSIrs_{Temin2}$ (3, 6) acquisitions. Standard deviation (indicated by σ as well as a gray color wash) and mean difference of the reference, 98th percentile of $RSIrs_{TEmin1}$, to the 98th percentile of $RSIrs_{TE90}$, $RSIrs_{TEmin2}$, and $RSIrs_{TE90corr}$ ($\Delta RSIrs$) indicating model bias. Black dashed lines indicate hypothetical perfect relation.

bration, the disparity between the 98th percentile of $RSIrs_{TE90}$ and $RSIrs_{TEmin1}$ was 2.28 ± 2.06SI ($p < 0.01$), more than 4 times larger than the difference between repeated acquisitions at the same TE. Following calibration, this average difference improved to -1.03SI ($p < 0.01$), signifying a 55% reduction in absolute error.

Figure S2 presents the 98th percentile of $RSIrs_{TEmin1}$, $RSIrs_{TEmin1corr}$, and $RSIrs_{TEmin2}$ within the prostate for each patient, comparing them to the reference (98th percentile of $RSIrs_{TE90}$), when TE90 is utilized as the reference sequence for calibration instead of TE_{min1}.

The threshold defined by the Youden index for the classification of csPCa was determined to be 8.94SI. $RSIrs_{TEmin1}$ has a sensitivity of 66% and a specificity of 72%. Prior to calibration, $RSIrs_{TE90}$ exhibits a low sensitivity (44%) coupled with high specificity (88%). Postcalibration, $RSIrs_{TE90corr}$ performs more similarly to the reference (sensitivity 73%, specificity 61%) see Figure S3.

4 | DISCUSSION

We present a straightforward, physics-based, method for calibration between different echo times. The calibration method demonstrated an improvement of inherent bias between $RSIrs_{TE90}$ and $RSIrs_{TEmin1}$. Residual error (in the 98th percentile of RSIrs) after calibration was 72% percent smaller in prostates without csPCa and 55% smaller in prostates with csPCa. The range between the 95th and 99th percentile of RSIrs proved to be a sufficient fitting range to avoid the impact of artifacts and voxels with no signal in lower percentiles, see Figure S5B.

A significant difference between $RSIrs_{TEmin1}$ and $RSIrs_{TEmin2}$ was observed in two acquisitions with identical imaging parameters acquired only a few minutes after each other without the patient leaving the scanner. Possible explanations for these changes could be explained by patient motion, changes in rectal gas, and hardware factors like pre-scan signal normalization or

gradient heating. These factors add complexity to the calibration process but also define the limits of achievable correspondence between scans. The absolute differences between the 98th percentile of $RSIrs_{TEmin1}$ and $RSIrs_{TEmin2}$ were larger for grade groups 4 and 5, as shown in Figure S4. The presented numbers reflect increased uncertainty in higher grade groups, making calibration for csPCa more challenging.

Due to the impact of noise in low percentiles and artifacts in high percentiles, concentrating on the 95th to 99th percentile is reasonable for the clinical use case of detection of csPCa, where the highest RSIrs values in a patient's prostate are known to drive quantitative performance of csPCa detection at the patient level.[18,19] We note, though, that a focus on calibrating high values may imply relatively poorer calibration in voxels with lower values. The clinical utility of values with near-zero values is unclear, so this may not be consequential in practice. Moreover, prostate images after calibration suggest the proposed method improves consistency with reference images (Figure 1, Figure 2).

An important limitation of this study is that the method solely addresses variations in echo time. Another limitation of the present work is reliance on data from a single institution and scanner manufacturer. To establish calibration across scanners from different manufacturers and accommodate changes in imaging parameters such as field strength and *b*-values, more sophisticated techniques like histogram matching[24,25] or the incorporation of machine learning methodologies[26] would be necessary. The study demonstrates the feasibility of a straightforward calibration method that accounts for echo time differences. However, since we did not compare different MRI manufacturers, we cannot assume the same scaling factors apply universally. To extend this methodology to other disease sites, imaging parameters, or scanners, a new linear regression model would need to be developed due to the lack of reliable diffusion phantoms. Nevertheless, a smaller sample size should suffice to determine a reliable scaling factor. As shown in Figure S5A, with a sample size of 35, the entire 95% confidence interval for the scaling factor is within 2% of the point estimate for the full dataset.

The present study is instructive, though, as it reveals that even minor variations of 15 ms in TE can result in significant differences in quantitative measurements that require careful calibration and demonstrate physics-based correction for these differences. Our findings may support protocol standardization, as much as possible, in the application of quantitative diffusion MRI to better ensure accurate and reliable results.

In conclusion, this study showed the feasibility of a straightforward calibration method to account for echo time differences for images acquired at the same scanner. DWI metrics are highly sensitive to changes in TE. A change of ~15 ms in TE resulted in errors 5-fold (csPCa cases) or 10-fold (benign prostates), compared to the errors incurred by simply repeating the acquisition with a consistent TE. The implementation of a simple linear calibration proves effective in generating comparable quantitative biomarker values across acquisitions with differing TE, resulting in a substantial reduction of TE-induced errors by 55% and 72% for csPCa and benign prostates, respectively.

AUTHOR CONTRIBUTIONS

Conception and design: Karoline Kallis, Tyler M. Seibert. *Administrative support*: Christopher C. Conlin, Courtney Ollison, Anders M. Dale, Tyler M. Seibert. *Provision of study materials or patients*: Karoline Kallis, Courtney Ollison, Anders M. Dale, Michael E. Hahn, Rebecca Rakow-Penner, Tyler M. Seibert. *Collection and assembly of data*: Karoline Kallis, Courtney Ollison, Christopher C. Conlin. *Data analysis and interpretation*: Karoline Kallis, Christopher C. Conlin, Anders M. Dale, Tyler M. Seibert. *Manuscript writing*: All authors. *Final approval of manuscript*: All authors

ACKNOWLEDGMENTS

This work was supported, in part, by the National Institutes of Health (NIH/NIBIB K08EB026503, NIH UL1TR000100), the American Society for Radiation Oncology, the Prostate Cancer Foundation, and the Department of Defense (DOD/CDMRP PC220278).

CONFLICT OF INTEREST STATEMENT

A.M.D. is a Founder of and holds equity in CorTechs Labs, Inc., and serves on its Scientific Advisory Board. He is a member of the Scientific Advisory Board of Human Longevity, Inc., and receives funding through research agreements with General Electric Healthcare. RRP is a consultant for Human Longevity, Inc. She also receives funding through research grants from GE Healthcare and Imagine Scientific to UC San Diego; she has an equity interest in CorTechs Labs, Inc. and serves on its Scientific Advisory Board. She also has an equity interest in CureMetrix. TMS reports honoraria from Multimodal Imaging Services Corporation, Varian Medical Systems, Janssen, and WebMD; he has an equity interest in CorTechs Labs, Inc. and serves on its Scientific Advisory Board. These companies might potentially benefit from the research results. The terms of the above arrangements have been reviewed and approved by the University of California San Diego in accordance with its conflict-of-interest policies.

REFERENCES

1. Siegel RL, Miller KD, Wagle NS, et al. Cancer statistics, 2023. *CA Cancer J Clin*. 2023;73:17-48.
2. Bengtsson J, Thimansson E, Baubeta E, et al. Correlation between ADC, ADC ratio, and Gleason Grade group in prostate cancer patients undergoing radical prostatectomy: retrospective multicenter study with different MRI scanners. *Front Oncol*. 2023;13:1079040.

3. Turkbey B, Rosenkrantz AB, Haider MA, et al. Prostate imaging reporting and data system version 2.1: 2019 update of prostate imaging reporting and data system version 2. *Eur Urol*. 2019;76:340-351.
4. Le Bihan D. Apparent diffusion coefficient and beyond: what diffusion MR imaging can tell us about tissue structure. *Radiology*. 2013;268:318-322.
5. Riches SF, Hawtin K, Charles-Edwards EM, et al. Diffusion-weighted imaging of the prostate and rectal wall: comparison of biexponential and monoexponential modelled diffusion and associated perfusion coefficients. *NMR Biomed*. 2009;22:318-325.
6. Le Bihan D, Breton E, Lallemand D, et al. Separation of diffusion and perfusion in intravoxel incoherent motion MR imaging. *Radiology*. 1988;168:497-505.
7. Rosenkrantz AB, Sigmund EE, Johnson G, et al. Prostate cancer: feasibility and preliminary experience of a diffusional kurtosis model for detection and assessment of aggressiveness of peripheral zone cancer. *Radiology*. 2012;264:126-135.
8. Si Y, Liu R-B. Diagnostic performance of monoexponential dwi versus diffusion kurtosis imaging in prostate cancer: a systematic review and meta-analysis. *AJR Am J Roentgenol*. 2018;211:358-368.
9. Panagiotaki E, Chan RW, Dikaios N, et al. Microstructural characterization of normal and malignant human prostate tissue with vascular, extracellular, and restricted diffusion for cytometry in tumours magnetic resonance imaging. *Invest Radiol*. 2015;50:218-227.
10. Johnston EW, Bonet-Carne E, Ferizi U, et al. VERDICT MRI for prostate cancer: intracellular volume fraction versus apparent diffusion coefficient. *Radiology*. 2019;291:391-397.
11. Singh S, Rogers H, Kanber B, et al. Avoiding unnecessary biopsy after multiparametric prostate MRI with VERDICT analysis: the INNOVATE study. *Radiology*. 2022;305:212536.
12. Chatterjee A, Watson G, Myint E, et al. Changes in epithelium, stroma, and lumen space correlate more strongly with Gleason pattern and are stronger predictors of prostate adc changes than cellularity metrics. *Radiology*. 2015;277:751-762.
13. Sadinski M, Karczmar G, Peng Y, et al. Pilot study of the use of hybrid multidimensional T2-weighted imaging-DWI for the diagnosis of prostate cancer and evaluation of Gleason score. *AJR Am J Roentgenol*. 2016;207:592-598.
14. Chatterjee A, Bourne RM, Wang S, et al. Diagnosis of prostate cancer with noninvasive estimation of prostate tissue composition by using hybrid multidimensional MR imaging: a feasibility study. *Radiology*. 2018;287:864-873.
15. Lee GH, Chatterjee A, Karademir I, et al. Comparing radiologist performance in diagnosing clinically significant prostate cancer with multiparametric versus hybrid multidimensional MRI. *Radiology*. 2022;305:399-407.
16. Brunsing RL, Schenker-Ahmed NM, White NS, et al. Restriction spectrum imaging: an evolving imaging biomarker in prostate MRI. *J Magn Reson Imaging*. 2017;45:323-336.
17. Conlin CC, Feng CH, Rodriguez-Soto AE, et al. Improved characterization of diffusion in normal and cancerous prostate tissue through optimization of multicompartmental signal models. *J Magn Reson Imaging*. 2021;53:628-639.
18. Feng CH, Conlin CC, Batra K, et al. Voxel-level classification of prostate cancer on magnetic resonance imaging: improving accuracy using four-compartment restriction spectrum imaging. *J Magn Reson Imaging*. 2021;54:975-984.
19. Zhong AY, Digma LA, Hussain T, et al. Automated patient-level prostate cancer detection with quantitative diffusion magnetic resonance imaging. *Eur Urol Open Sci*. 2023;47:20-28.
20. White NS, McDonald C, McDonald CR, et al. Diffusion-weighted imaging in cancer: physical foundations and applications of restriction spectrum imaging. *Cancer Res*. 2014;74:4638-4652.
21. Egnell L, Jerome NP, Andreassen MMS, et al. Effects of echo time on IVIM quantifications of locally advanced breast cancer in clinical diffusion-weighted MRI at 3 T. *NMR Biomed*. 2022;35:e4654.
22. Holland D, Kuperman JM, Dale AM. Efficient correction of inhomogeneous static magnetic field-induced distortion in echo planar imaging. *NeuroImage*. 2010;50:175-183.
23. Zhuang J, Hrabe J, Kangarlu A, et al. Correction of eddy-current distortions in diffusion tensor images using the known directions and strengths of diffusion gradients. *J Magn Reson Imaging*. 2006;24:1188-1193.
24. Jäger F, Hornegger J. Nonrigid registration of joint histograms for intensity standardization in magnetic resonance imaging. *IEEE Trans Med Imaging*. 2009;28:137-150.
25. Ceranka J, Lecouvet F, Michoux N, et al. Comparison of intra- and inter-patient intensity standardization methods for multi-parametric whole-body MRI. *Biomed Phys Eng Express*. 2023;9:035028.
26. Torbati ME, Tudorascu DL, Minhas DS, et al. Multi-scanner harmonization of paired neuroimaging data via structure preserving embedding learning. In: IEEE Int Conf Comput Vis Workshop IEEE Int Conf Comput Vis *2021*. IEEE; 2021:3277-3286.

SUPPORTING INFORMATION

Additional supporting information can be found online in the Supporting Information section at the end of this article.

How to cite this article: Kallis K, Conlin CC, Ollison C, et al. Quantitative MRI biomarker for classification of clinically significant prostate cancer: Calibration for reproducibility across echo times. *J Appl Clin Med Phys*. 2024;25:e14514. https://doi.org/10.1002/acm2.14514